

# MOBIUS: A Multi-Modal Bipedal Robot that can Walk, Crawl, Climb, and Roll

Alexander Schperberg<sup>1\*</sup>, Yusuke Tanaka<sup>2\*</sup>, Stefano Di Cairano<sup>1</sup> and Dennis Hong<sup>2</sup>

**Abstract**—This paper presents the MOBIUS platform, a bipedal robot capable of walking, crawling, climbing, and rolling. MOBIUS features four limbs, two 6-DoF arms with two-finger grippers for manipulation and climbing, and two 4-DoF legs for locomotion—enabling smooth transitions across diverse terrains without reconfiguration. A hybrid control architecture combines reinforcement learning for locomotion and admittance control enhanced for safety by a Reference Governor and auto-tuning toward compliant contact interactions during manipulation. A high-level MIQCP planner autonomously selects locomotion modes to balance stability and energy efficiency. Hardware experiments demonstrate robust gait transitions, dynamic climbing, and full-body load support via pinch grasp. Overall, MOBIUS demonstrates the importance of tight integration between morphology, high-level planning, and control to enable mobile locomanipulation and grasping, substantially expanding its interaction capabilities, workspace, and traversability.

## I. INTRODUCTION

Legged robots offer strong versatility for navigating complex, human-made environments, motivating applications in search and rescue, inspection, and exploration. Prior work has produced highly capable but largely specialized platforms, including bipeds (Feng et al. [12], Gong et al. [15], Castillo et al. [7]), quadrupeds (Bellegarda et al. [3], Hutter et al. [18], Seok et al. [34], Bouman et al. [5]), and hopping or jumping robots (Raibert et al. [28], Yim and Fearing [43]). Parallel advances in manipulation have enabled loco-grasping behaviors (Shi et al. [35], Fu et al. [13], Su et al. [36], Gong et al. [14]), but only a small number of systems address the extreme case of free climbing in discrete, vertical environments. Most climbing robots rely on adhesion (Kim et al. [20], Saunders et al. [30], Austin et al. [2]) or passive spine-based grasping Parness et al. [24], Uno et al. [41], Nagaoka et al. [23]), which limits dexterity, and dynamic climbing. While SCALER (Tanaka et al. [38]) demonstrates grasping-based climbing under Earth gravity, it sacrifices general ground mobility. More broadly, existing legged robots typically excel in a single locomotion regime, limiting adaptability across continuous and discrete terrain.

To address these limitations, we introduce MOBIUS (**M**ulti-modal **O**perations **B**ipedal **I**ntelligent **U**rban **S**

<sup>1</sup>A. Schperberg, and S. Di Cairano are with Mitsubishi Electric Research Laboratories (MERL), Cambridge, MA 02139 USA (email: schperberg@merl.com, dicairano@ieee.org).

<sup>2</sup>Y. Tanaka, and D. Hong are with the Robotics and Mechanisms Laboratory, Department of Mechanical and Aerospace Engineering, University of California, Los Angeles, CA, 90095, USA (email: yusuketanaka@g.ucla.edu, dennishong@g.ucla.edu).

\*Denotes equal contribution.

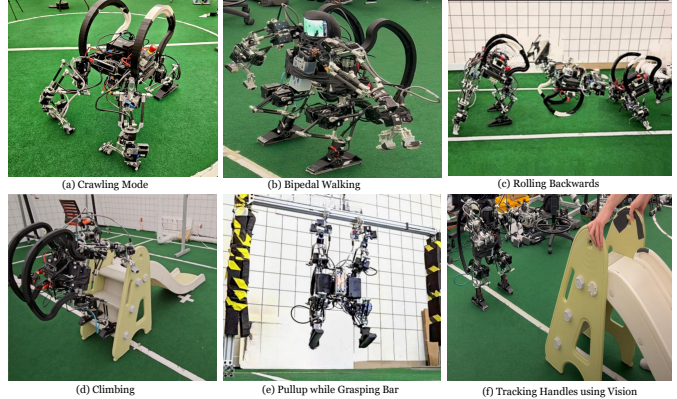


Fig. 1: MOBIUS: Multi-modal Operations Bipedal Intelligent Urban Scout.

unified platform capable of bipedal walking, crawling, rolling, and dynamic free climbing. MOBIUS transitions seamlessly between modes to balance efficiency, stability, and manipulation. Equipped with two grippers (Tanaka et al. [37]), it can support its full body weight and perform pinching-based pull-ups. To the best of our knowledge, MOBIUS is the first bipedal robot using finger grippers to achieve walking, crawling, free-climbing as defined by Bretl [6], rolling, and pull-ups within a single morphology without mechanical re-configuration.

Overall, we provide the following **contributions**:

- 1) A novel multi-modal robot combining two 6-DoF dexterous arms with two-finger grippers and two 4-DoF legs, with integrated rails for fall protection and rolling.
- 2) A unified morphology enabling bipedal walking, crawling, rolling, vertical free climbing, and pull-up maneuvers under Earth gravity.
- 3) An adaptive admittance controller with a Reference Governor for safety in contact-rich scenarios.
- 4) A MIQCP-based high-level planner for locomotion mode selection.
- 5) Extensive hardware validation demonstrating multi-modal locomotion, transitions, climbing, and pull-ups.

## A. Paper Organization

The paper is organized as follows. Related works on multi-modal robots, covering both hardware and software aspects, are presented in Sec. II. The MOBIUS hardware is described in Sec. III, including design challenges such as multi-modality requirements, performance–robustness trade-offs, and integration and scalability considerations. Further details on the

limb and gripper design, actuator selection, fatigue analysis, and reliability are left as Supplementary Material (Sec. A of Appendix). A summary of locomotion modes is given in Sec. III-C. The software architecture (Fig. 4) covers RL-based planning and control (Sec. IV-A), where details on the model-based MPC baseline (used to compare against RL) is given in Sec. C of Appendix. Additional modules include the force controller (Sec. IV-B), and high-level multimodal planner (Sec. IV-C). Other modules such as our state estimator and visual-servo controller are in the Supplementary Material (Sec. G and Sec. H of Appendix respectively). Finally, Sec. V presents simulation and hardware integration and extensive experimental results on locomotion, climbing, pull-ups, force control, comparisons between MPC and RL, multimodal planning, and visual-servo tracking.

## II. RELATED WORK

We review prior work from two perspectives: (i) hardware designs enabling multi-modal locomotion in Sec. II-1, and (ii) planning and control architectures for coordinating multiple locomotion modes in Sec. II-2.

1) *Hardware for Multi-Modality*: Multi-modal robots leverage multiple locomotion strategies within a single platform to improve adaptability. Harpy (Dangol et al. [10]) and LEONARDO (Kim et al. [19]) combine bipedal walking with torso-mounted thrusters to overcome obstacles via short-duration flight. AuxBots (Chin et al. [9]) achieve flipper-style locomotion through modular, volume-changing assemblies, while origami-inspired robots (Chen et al. [8]) use shape morphing and variable stiffness for transitions between rigid and soft locomotion. ALPHRED (Hooks et al. [17]) employs a radially symmetric quadrupedal morphology to enable simultaneous locomotion and dual-arm manipulation. RiSE (Saunders et al. [30]) uses compliant legs with micro-spine feet for vertical climbing on rough surfaces. ANYmal-Wheel (Bjelonic et al. [4]) integrates legged and wheeled locomotion for efficient mode switching, and GOAT-SR (Polzin et al. [26]) supports driving, rolling, and swimming via active and passive deformation. The soft wheel-leg robot (Ai et al. [1]) combines pneumatic actuation and wheel-like appendages to traverse constrained environments through rolling and crawling. Most prior systems rely on mechanical reconfiguration or mode-specific appendages, increasing complexity and mass. In contrast, MOBIUS achieves walking, crawling, climbing, and rolling with a single unified morphology and no physical reconfiguration. Its limbs equipped with two-finger spine-based grippers (Tanaka et al. [37]) serve both as compliant contacts and high-force grasping tools. While pull-up behaviors have been demonstrated on limited platforms such as ARMStrong Dex (Korea Atomic Energy Research Institute [21]), MOBIUS is the first mid- to large-scale biped to perform a pinch-grasp pull-up from a full dead-hang configuration.

2) *Multi-Modal Planning and Control*: Coordinating multiple locomotion modes require control frameworks that handle discontinuous dynamics and varying contact conditions. Harpy (Dangol et al. [10]) regulates ground reaction forces

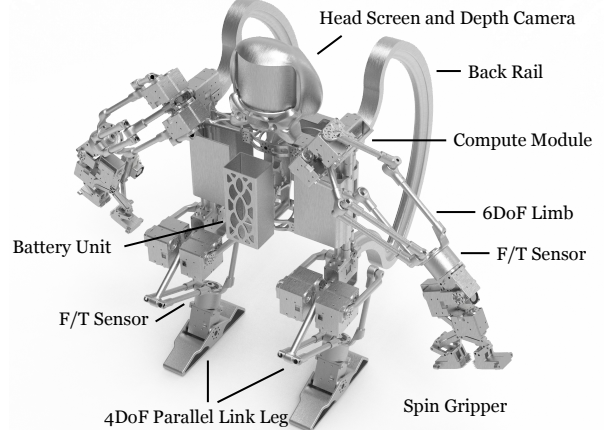


Fig. 2: MOBIUS overall structure rendering.

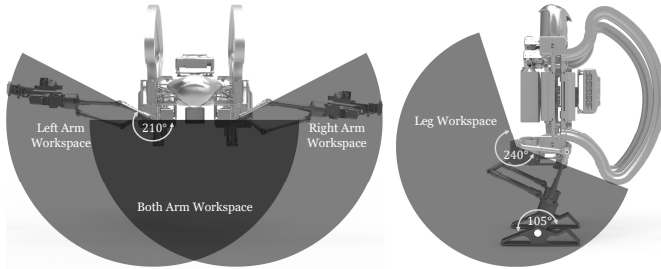
via thrusters, while AuxBots (Chin et al. [9]) control inter-module distances for efficient flipper motion. Origami-based robots (Chen et al. [8]) analytically compute variable-stiffness joint configurations to switch between walking, crawling, and grasping. RiSE (Saunders et al. [30]) adapts climbing and walking behaviors using distributed sensing and contact feedback. ANYmal-Wheel (Bjelonic et al. [4]) employs hierarchical whole-body control with ZMP-based optimization and nonholonomic rolling constraints. The soft wheel-leg robot (Ai et al. [1]) coordinates pneumatic and wheel actuation to switch between crawling strategies. Hybrid learning-based approaches such as from Yu and Rosendo [44] use Automated Residual Reinforcement Learning to transition between quadruped and bipedal gaits, combining classical control with model-free RL methods including SAC and TD3.

Building on these ideas, MOBIUS employs a unified hybrid control stack. Model-free RL governs bipedal and crawling behaviors, while a model-based approach is used for contact-rich tasks through combining an adaptive admittance control with a Reference Governor (Schperberg et al. [33]) for safety. A high-level MIQCP planner autonomously selects locomotion modes to minimize energy subject to reachability and terrain constraints. This integration enables autonomous transitions across modes without manual triggering or hardware reconfiguration.

## III. HARDWARE AND SYSTEM MECHANISMS

### A. Design Objectives and Challenges

MOBIUS builds upon the mechanism design from Tanaka et al. [38] to support fundamentally different locomotion regimes, including bipedal walking, crawling, rolling, and vertical climbing. Unlike that mechanisms design, which is optimized for climbing, MOBIUS must support its full body weight on a single limb during bipedal walking while maintaining sufficient swing velocity and stability. This imposes conflicting requirements on kinematics, force capability, and actuator selection. To address this, MOBIUS adopts limb kinematics that balance velocity and force isotropy at nominal



(a) MOBIUS limb workspace in the top view with (b) MOBIUS leg workspace in the 210° range.

Fig. 3: Kinematic ranges of the MOBIUS limb modules.

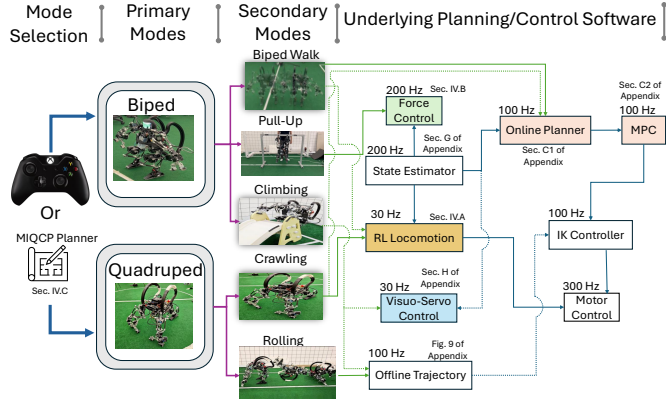


Fig. 4: We demonstrate the overall flowchart, from user primary mode selection, to the secondary modes associated with each primary mode. The modes can be selected either by the user through a joystick, or autonomously, if given a 2D map of the environment with relevant features, using our high level MILP-based planner (see Sec. IV-C). The underlying planners and controllers corresponding to each secondary mode are shown on the right side of the figure, along with their operating frequencies and references to the sections of this work where each module is discussed.

bipedal and crawling configurations, while retaining dexterous arm linkage for climbing and manipulation. The gripper serves as both a dexterous end-effector and a load-bearing contact during crawling, enabling seamless transitions between manipulation and locomotion without mechanical reconfiguration.

### B. Mechanical Architecture Overview

MOBIUS employs two 6-DoF arms with two-finger spine-based grippers and two 4-DoF legs with flat feet (Fig. 2). MOBIUS hybrid parallel mechanism linkages help to withstand repeated impact loads during bipedal locomotion while being capable of power-intensive and dexterous contact-rich climbing. Curved back rails passively guide the robot into recoverable postures following backward falls, reducing control and workspace requirements (Fig. 3). Further details on limb kinematics and Jacobian properties, fatigue analysis, and end-effector design choice is detailed in Sec. A of Appendix.

### C. Multi-Modal Locomotion Capabilities

MOBIUS supports five primary capabilities: bipedal walking, crawling, rolling, vertical mobility, and autonomous transitions between modes. Each mode offers distinct trade-offs

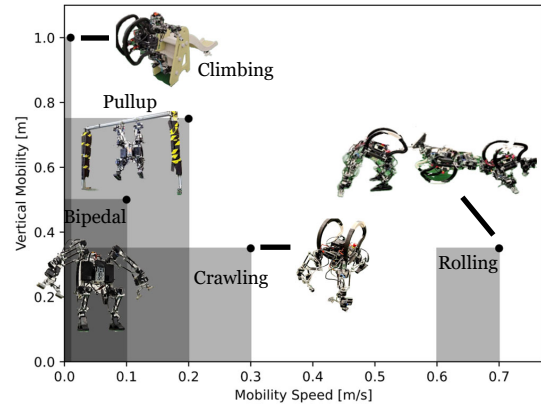


Fig. 5: MOBIUS mobility envelope across locomotion modes.

in speed, stability, and energy efficiency, enabling task- and terrain-dependent operation (Fig. 5).

In bipedal mode, MOBIUS walks omnidirectionally while freeing its arms for manipulation or climbing. Crawling uses all four limbs to maximize stability on rough terrain. Back-mounted rails enable backward rolling, providing both fall protection and an energy-efficient locomotion mode. Vertical mobility is achieved through grasping-based climbing and pinch-grasp pull-ups using the grippers, enabling traversal of discrete structures such as ladders and bars. Finally, MOBIUS can transitions between modes, including fall recovery and standing-to-crawling transitions (and vice-versa), and crawling to rolling. We visually show and detail these transition modes in Sec. I, and Fig. 9 of Appendix.

## IV. SOFTWARE ARCHITECTURES FOR PLANNING AND CONTROL

The full software architecture and locomotion modes are shown in Fig. 4, with pointers to the relevant subsections describing them. For ablations, we compare a reinforcement learning approach (Sec. IV-A) against a model-based baseline for biped and crawling locomotion (baseline implementation details are in Sec. C of Appendix).

### A. Reinforcement Learning for Planning and Control

Compared to conventional bipeds and humanoids, MOBIUS has forearms that are 55% heavier than its lower body. While this asymmetry facilitates transitions between bipedal and crawling modes, it significantly complicates bipedal locomotion due to uneven mass distribution and arm-induced momentum. Although model-based control has proven effective for many bipeds and quadrupeds (Raibert [27], Kuindersma et al. [22]), it is insufficient for MOBIUS due to poorly characterized dynamics. We therefore adopt a fully model-free reinforcement learning (RL) approach, which has shown strong performance in prior work (Tsounis et al. [40]), and avoid reference trajectories or motion priors (Vollenweider et al. [42], Escontrela et al. [11]).

1) *Problem Definition*: The RL controller enables MOBIUS to track user joystick commands and is primarily used for bipedal locomotion, where stability is most challenging. Crawling is inherently stable and follows commanded velocities using the model-based controller described in Sec. C of Appendix (although we also show comparisons between RL and model-based for crawling in Fig. 8). Locomotion is formulated as a Partially Observable Markov Decision Process (POMDP), and policies are trained using Proximal Policy Optimization (PPO). Training proceeds in two stages: first on flat terrain, then fine-tuned on rough terrain. Hyperparameters, training durations, domain randomization, and disturbances are detailed in Sec. B of Appendix.

2) *Observation and Action*: The observation vector is defined as

$$\mathbf{O}_t = [\mathbf{X}_t, \Theta_t, \mathbf{A}_{t-1}, \mathbf{v}_{xy}^{\text{des}}, \omega_z^{\text{des}}, \mathbf{O}_{t-N:t-1}],$$

where  $\mathbf{X}$  represents the estimated trunk state, including orientation, angular velocity, and linear velocity;  $\Theta$  denotes joint encoder values;  $\mathbf{A}_{t-1}$  is the previous action; and  $\mathbf{v}_{xy}^{\text{des}}$  and  $\omega_z^{\text{des}}$  are desired linear and angular velocities. The action space consists of target joint positions, with dimensions depending on locomotion mode. A history of  $N = 15$  observations is included, resulting in observation dimensions of  $\mathbb{R}^{416}$  for bipedal mode and  $\mathbb{R}^{608}$  for crawling.

Actions are filtered using a moving average to improve smoothness for hardware execution:

$$\Theta_{\text{action}} = \Theta_{\text{default}} + \left( \frac{1}{n_{\text{actions}}} \sum_{i=1}^{n_{\text{actions}}} \mathbf{A}_{t-i} \right) a_{\text{scale}}, \quad (1)$$

where  $\Theta_{\text{default}}$  is the nominal pose and  $a_{\text{scale}}$  is a scaling factor.

3) *Reward Function*: The reward function employed balances stability, tracking accuracy, and smoothness. Specifically, it penalizes vertical motion, pitch and roll rates, large action changes, foot slip, and short episodes, while rewarding planar velocity tracking, yaw-rate tracking, standing still at low commanded speeds, and sufficient foot air time to promote proper stepping. See Sec. B of Appendix for details on reward and penalty functions.

## B. Grasping Force Control

MOBIUS can lift its full body weight using a two-finger gripper. To keep grasping smooth and safely, both for task execution and under external disturbances (e.g., pushing and pulling), we introduce compliance via force control. We employ an admittance controller that maps measured wrench to a desired motion (change in position). This is suitable for robots with position-controlled actuators that must still behave compliantly during contact. For clarity, we refer to the end-effector as the *fingertip* and the wrist as the *gripper base*.

We build on the auto-tuning admittance framework from Schperberg et al. [31], which adapts controller gains online to track position and wrench profiles, minimize slip, and avoid kinematic singularities and combine it with adding safety guarantees through a Reference Governor as shown

in Schperberg et al. [33]. The overall architecture is shown in Fig. 6. Details of the auto-tuning module and ablations are found in Schperberg et al. [31]; we summarize the core controller here.

The admittance dynamics are:

$$\ddot{\mathbf{x}} = \mathbf{M}_d^{-1} \left( -\mathbf{D}_d \mathbf{V}_{\text{cur}} - \mathbf{K}_d (\mathbf{X}_{\text{cur}} - \mathbf{X}_{\text{ref}}) + \mathbf{K}_f (\mathcal{W}_{\text{meas}} - \mathcal{W}_{\text{ref}}) \right), \quad (2)$$

where  $\mathcal{W}_{\text{meas}}, \mathcal{W}_{\text{ref}} \in \mathbb{R}^{6k}$  are measured and desired wrenches at fingertip or contact  $k$ , with  $\mathcal{W} = [\mathbf{f}^\top, \boldsymbol{\tau}^\top]^\top$  ( $\mathbf{f} \in \mathbb{R}^{3k}$  forces and  $\boldsymbol{\tau} \in \mathbb{R}^{3k}$  torques).  $\mathbf{M}_d$  (invertible),  $\mathbf{D}_d$ , and  $\mathbf{K}_d \in \mathbb{R}^{6k \times 6k}$  are diagonal desired mass, damping, and stiffness matrices, and  $\mathbf{K}_f \in \mathbb{R}^{6k \times 6k}$  scales wrench sensitivity.  $\mathbf{X}_{\text{cur}}$  and  $\mathbf{V}_{\text{cur}}$  are fingertip pose and velocity with  $\mathbf{X}_{\text{cur}} = [\mathbf{p}^\top, \Theta^\top]^\top$ , where  $\mathbf{p} \in \mathbb{R}^{3k}$  and  $\Theta \in \mathbb{R}^{3k}$  is the fingertip position and orientation.  $\mathbf{X}_{\text{ref}}$  is the reference trajectory, and Euler-angle differencing is handled as in Piovan and Bullo [25]. The resulting  $\ddot{\mathbf{x}}$  is discretized using Euler integration to obtain  $\mathbf{x}$ , then mapped to joint commands via inverse kinematics,  $f_{\text{kin}}^{-1}(\mathbf{x}) = \theta_{\text{joint}}$  angles, and sent to low-level motor controllers.

1) *Reference Governor for Safety Guarantees*: Force control must respect state and control limits while maintaining performance. We enforce safety using a Reference Governor (RG), an add-on module that modifies the commanded reference in real time to avoid constraint violations while remaining as close as possible to the original input. The RG is based on the Maximal Output Admissible Set (MOAS), defined as the set of initial states and references for which constraints are never violated:

$$\mathcal{O}_\infty = \{(x_0, v) \mid y(t) \in \mathcal{Y} \ \forall t \geq 0\}, \quad (3)$$

where  $x_0$  is the initial state,  $v$  the reference,  $y(t)$  the system output, and  $\mathcal{Y}$  the admissible output set determined by safety and performance limits.

2) *Control Law for Reference Governor*: The RG feasibility check uses the closed-loop control law

$$\mathbf{u}(t) = \ddot{\mathbf{x}} - \mathbf{K}_{I_x} \mathbf{z}_x - \mathbf{K}_{I_f} \mathbf{z}_f, \quad (4)$$

where  $\ddot{\mathbf{x}}$  is from (2),  $\mathbf{z}_x, \mathbf{z}_f$  are integral error terms for position and wrench, and  $\mathbf{K}_{I_x}, \mathbf{K}_{I_f}$  are integral gains that promote smoothness. To prevent windup under saturation or large disturbances, we reset integrators when acceleration exceeds bounds:

$$\text{if } |\ddot{\mathbf{x}}| > \ddot{\mathbf{x}}_{\text{max}} \Rightarrow \mathbf{z}_x = \mathbf{z}_f = 0.$$

We compute  $\mathcal{O}_\infty$  offline by simulating trajectories over a finite horizon using second-order Euler integration. For each sampled  $(\mathbf{x}_{\text{cur}}, \mathbf{v}_{\text{cur}}, \mathbf{x}_{\text{ref}}, \mathbf{W}_{\text{cur}}, \mathbf{W}_{\text{ref}})$ , we roll out (4). Samples whose trajectories satisfy position, velocity, and wrench constraints are retained in  $\mathcal{O}_\infty$ . We apply this per axis (x, y, z) for position, velocity, and force, and include torque about the gripper-base normal. Full algorithmic details are in Sec. D of Appendix.

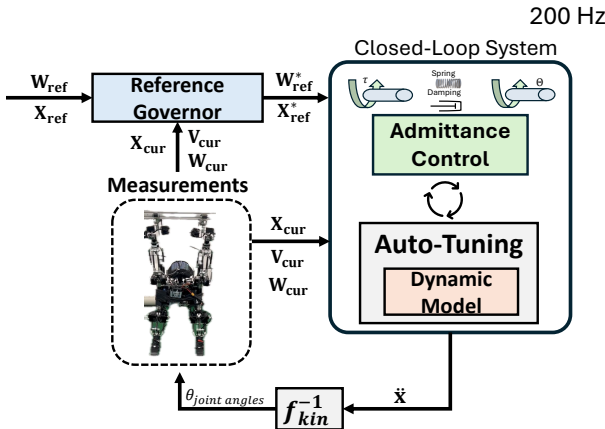


Fig. 6: The force controller used during the pull-up mode is demonstrated. It consists of an admittance controller where the gains are adapted during online operation as done in Schperberg et al. [31]. To promote safety guarantees during force control, we expand that work with the addition of a Reference Governor (RG), outlined in Sec. IV-B1. The RG takes as input the current state, and desired reference, and outputs a modified reference (if necessary) to steer the system into regions of stability based on the maximal output admissible set.

3) *Employing Reference Governor*: Given  $\mathcal{O}_\infty$ , the RG modifies the reference setpoint at the current state so that a feasible control sequence exists and constraints are satisfied for all future time. To enable fast online checks, we store discrete samples of  $\mathcal{O}_\infty$  in a KD-Tree for logarithmic-time nearest-neighbor queries. For a query  $o_q$ , if  $o_q \notin \mathcal{O}_\infty$ , we find the closest admissible point

$$o^* = \arg \min_{o \in \mathcal{O}_\infty} \|o - o_q\|, \quad (5)$$

with  $o = [\mathbf{x}, \mathbf{v}, \mathbf{x}_{\text{ref}}, \mathbf{W}, \mathbf{W}_{\text{ref}}]$ . We keep  $(\mathbf{x}, \mathbf{v}, \mathbf{W})$  fixed and replace the references with  $(\mathbf{x}_{\text{ref}}^*, \mathbf{W}_{\text{ref}}^*)$  so the system is steered back into the admissible set.

### C. High-Level Multi-Modal Planning

We present a high-level planner that lets a multi-modal robot optimize its trajectory while switching modes online. The problem is formulated as a Mixed Integer Quadratic Constraint Programming (MIQCP) problem, enabling joint optimization of grid-based path planning and discrete mode selection. The objective balances exploration, goal reaching within a time horizon, and energy or stability costs, while terrain and obstacle constraints ensure safe, feasible navigation.

1) *MIQCP and Mixed Integer Formulation*: MOBIUS can transition between crawling, biped, and rolling to satisfy task demands. Our MIQCP planner exploits this by selecting both a mode sequence and a trajectory, using big-M to handle *if-then* logic. The task is to move from a start to a goal within  $T$  steps, avoid obstacles, and maximize exploration of a discretized  $N_{\text{grid}} \times N_{\text{grid}}$  2D map. While the task is solvable in a single mode, multi-modal planning yields higher coverage and efficiency (Sec. V-E).

The robot state on the grid is represented by variables  $x(t, 0)$  and  $x(t, 1)$  for planar position, and binary variables  $V(i, j)$  encode visited cells and modes. Movement propagation

depends on the active mode, with per-mode step sets for  $d(t)$ , and a one-hot constraint  $m$  enforces a single mode at each time. Full variable definitions, constraint interpretations, and analysis on hyper-parameter selections are given in Sec. E of Appendix.

2) *Terrain and Obstacle Handling*: We incorporate terrain-dependent mode constraints and obstacle avoidance into the MIQCP. Terrain regions are modeled as circles that activate binary indicators when the robot is inside them, and these indicators restrict allowable modes (e.g., crawling on rough terrain, biped on elevated-visibility regions). Obstacles are modeled as rectangles that the robot is forbidden to enter. See Sec. E in Appendix for the explicit constraint logic.

3) *Objective Functions and Trade-off*: The objective trades off exploration against goal reaching, and includes mode penalties to discourage costly modes unless needed:

$$\max_{V_{i,j}, x} \quad W_{\text{exp}} \sum_{i=0}^{N_{\text{grid}}-1} \sum_{j=0}^{N_{\text{grid}}-1} V_{i,j} - W_{\text{goal}} \|x_T - x_{\text{goal}}\|^2 \\ - \sum_{t=0}^{T-1} \sum_{k=1}^3 P_k m_k(t) \quad \text{s.t. (1) - (20), see Table I.}$$

Here  $W_{\text{exp}}$  and  $W_{\text{goal}}$  represent weight exploration and goal tracking, and  $P_k$  penalizes mode  $k$ . Crawling has the lowest penalty (most stable and efficient), biped is higher, and rolling is highest due to modeling the localization instability. This biases the planner toward crawling by default, biped when required by the task or terrain, and rolling only when large strides are needed to meet the horizon objective.

TABLE I: MIQCP Constraints (1)-(20)

Visiting Grid Constraints	
(1)	$z(t, i, j) \in \{0, 1\}$
(2)	$z_{\text{sum}}(i, j) = \sum_{t=0}^{T-1} z(t, i, j), \quad \forall i, j \in \{0, 1, \dots, N_{\text{grid}} - 1\}$
(3)	$V(i, j) \leq z_{\text{sum}}(i, j), \quad \forall i, j$
(4)	$V(i, j) \leq T \cdot V(i, j), \quad \forall i, j$
(5)	$x(t, 0) - i \geq -M(1 - z(t, i, j))$
(6)	$x(t, 1) - j \geq -M(1 - z(t, i, j))$
Propagation Update	
(7)	$x(t+1) = x(t) + d(t)$
Mode Types Constraints	
(8)	$m_1(t) = 1 \implies d(t) \in \{-1, 1\}$
(9)	$m_2(t) = 1 \implies d(t) \in \{-2, -1, 1, 2\}$
(10)	$m_3(t) = 1 \implies d(t) \in \{-3, 3\}$
(11)	$m_1(t) + m_2(t) + m_3(t) = 1$
Terrain Type Constraints	
(12)	$d_{\text{circle}} = (x(t, 0) - x_{\text{center}})^2 + (x(t, 1) - y_{\text{center}})^2$
(13)	$d_{\text{circle}} \leq r_{\text{circle}}^2 + M(1 - b_{\text{circle}}^k(t))$
(14)	$d_{\text{circle}} \geq r_{\text{circle}}^2 + \epsilon - Mb_{\text{circle}}^k(t)$
(15)	$m_k(t) \geq b_{\text{circle}}^k(t), \quad b_{\text{circle}}^k \in \{0, 1\}$
Obstacle Constraints	
(16)	$x(t, 0) \geq x_{\text{min}} + M(1 - b_1^{\text{rect}}(t))$
(17)	$x(t, 0) \leq x_{\text{max}} - M(1 - b_2^{\text{rect}}(t))$
(18)	$x(t, 1) \geq y_{\text{min}} + M(1 - b_3^{\text{rect}}(t))$
(19)	$x(t, 1) \leq y_{\text{max}} - M(1 - b_4^{\text{rect}}(t))$
(20)	$b_1^{\text{rect}}(t) + b_2^{\text{rect}}(t) + b_3^{\text{rect}}(t) + b_4^{\text{rect}}(t) \leq 3$

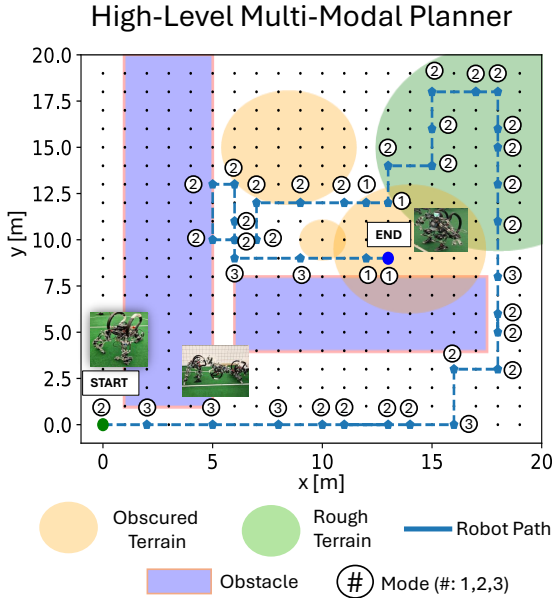


Fig. 7: We show one example map, along with the output of our MIQCP-based planner, where the output consist of connected waypoints, where each waypoint is designated with the desired robot mode selection, numbered from (1) to (3). Mode (1) means the robot must be in biped mode, mode (2) is crawling, and mode (3) is rolling. The solver aims to optimize for reaching the goal or end state within a limited time (or N points), achieve low energy consumption, visit as many cells as possible, avoid obstacles, and meet terrain requirements which may enforce being in one mode or another, see Sec. IV-C.

TABLE II: Maximum Locomotion Velocities

Mode	Biped Mode	Crawling Mode	Rolling Mode
Max velocity (m/s)	0.1	0.4	0.7

## V. EXPERIMENTAL RESULTS

### A. Simulation and Hardware Integration

The simulation-to-hardware integration uses policies trained in the high-fidelity MuJoCo (Todorov et al. [39]) simulation with domain randomization over mass ( $\mathcal{U}(-5.0, 5.0)$ kg), friction ( $\mathcal{U}(-0.3, 0.5)$ ), actuator gains/biases ( $\mathcal{U}(\pm 20)$ ), and observation delays. RL policies run at 60 Hz, outputting smoothed joint positions via a moving average, tracked by 300 Hz low-level PID motor controllers. For contact-rich tasks like pull-ups, an admittance controller with auto-tuning operates at 300 Hz to ensure compliant force tracking, while safety is enforced using a Reference Governor and a precomputed Maximal Output Admissible Set (MOAS). State estimation fuses the slower T265 VIO-SLAM (200 Hz) with the OptiState algorithm (Schperberg et al. [32]), enabling robust real-time control across all locomotion modes with zero-shot sim-to-real transfer. The visual-servo control module enables pre-manipulation positioning by tracking the slide's handle bars before climbing. An object detection model (Redmon et al. [29]) runs at 30 Hz, synchronized with the RGB-D camera, to estimate the centroid positions of the handles. The resulting reference positions are converted to joint angles using IK. For the high-level multi-modal planner, the MIQCP optimization can take approximately 10-11 seconds to solve on a 20 m by

20 m map for a 20 second trajectory. We use Gurobi (Gurobi Optimization, LLC [16]) as the optimization solver.

### B. Bipedal Locomotion Performance

We compare a model-based controller using online planning and MPC (Sec. C of Appendix) with a model-free RL policy (Sec. IV-A) for biped and crawling locomotion. To evaluate robustness, we apply increasing impulse velocity disturbances of 0.1 s duration to the robot's CoM during standing until failure occurs. The model-based controller fails at approximately 0.05 m/s disturbance, while the RL policy remains stable up to 0.25 m/s. This behavior is expected, as MOBIUS exhibits complex, asymmetric dynamics that are difficult to model accurately, leading to state propagation errors in MPC, whereas the RL policy implicitly captures these effects. The RL controller is further validated under height-map disturbances in simulation and in hardware experiments. We additionally compare velocity tracking performance on hardware for  $x$ ,  $y$ , and yaw motions (Fig. 8a), including lateral, forward, backward, and rotational commands. Target velocity is shown in green, with estimated velocities from the model-based controller (blue) and RL policy (red). The robot achieves up to 0.1 m/s laterally and 0.25 rad/s in yaw. Across all motions, the model-based approach exhibits higher tracking error, while the RL policy consistently improves accuracy. Although the RL policy shows slightly worse forward  $x$ -velocity tracking, the model-based controller induces larger errors in undesired  $y$  and yaw directions despite a zero velocity reference, indicating superior disturbance rejection and motion decoupling by the RL policy.

### C. Crawling Locomotion Analysis

A similar velocity tracking comparison between the model-based approach and RL is given for the crawling locomotion in Fig. 8b. Unlike bipedal locomotion, the model-based and RL approach provided more comparable results, although overall, for sideways, and backward motion, RL performed improved tracking. One reason the RL policy struggles with velocity tracking compared to biped locomotion, may be due to the complexity of contact dynamics introduced by using the robot's two gripper-equipped arms as front limbs. These grippers are not optimized for high-frequency ground contact, and the simulator may not accurately model their contact behavior, leading to discrepancies during sim-to-real transfer. Additionally, crawling locomotion operates at higher speeds than biped mode, making tracking more difficult due to increased dynamic effects. Specifically, crawling mode can reach up to 0.4 m/s in lateral directions and 0.6 rad/s in yaw direction. Finally, the asymmetry in limb morphology, two arms and two legs with different masses, kinematics, and end-effectors, introduces further modeling and control challenges not present in more uniform crawling locomotion.

### D. Rolling Locomotion

The rolling motion shares similar key points from transition from crawling to standing or biped mode, but before it reaches

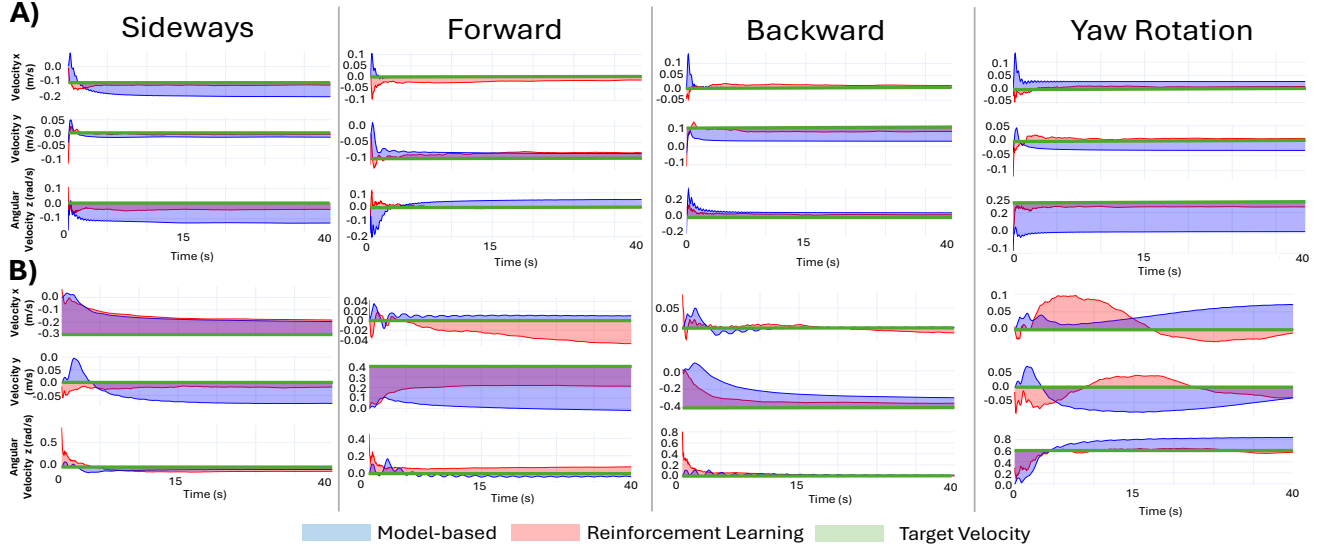


Fig. 8: We compare velocity tracking ability between biped mode shown in row (A) and crawling mode shown in row (B) using the baseline model-based approach, Sec. C of Appendix and using RL, Sec. IV-A for sideways, forward, backward, and yaw rotation motion. The velocity values for model-based is shown in blue, RL in red, and the target or reference velocity shown in green. For example, in the sideways motion for the biped mode, the target velocity in x is  $-0.1$  m/s, and  $0.0$  m/s in y and angular velocity (since we command the robot to go sideways only). Note, for our frame definition, the y-axis is pointed forwards.

the default standing pose, it jumps backward and uses the back rail to roll, as shown in Fig. 1c. This rolling motion is the fastest locomotion at  $0.7$  m/s, which is  $600.0$  % and  $75.0$  % faster than biped walking and crawling respectively. Nevertheless, although this motion is more energy-efficient compared to biped mode, it is the least stable as the motion cannot be perfectly controlled, particular during the roll where it passively (rather than actively) performs the motion using its back rails. This introduces errors for state estimation, where the robot cannot be tracked accurately.

#### E. Multi-Modal High-Level Planning Results

We evaluate our multi-modal high-level planner (Sec. IV-C) using the Energy per Visited Cell (EVC) metric. The planner aims to reach the goal while maximizing exploration and minimizing energy per visited grid cell. Energy per Visited cell is defined as the total energy expenditure (joint velocity  $\times$  joint torque) divided by the number of unique grid cells visited. Energy usage is computed from each locomotion mode's maximum velocity (Table II) and travel distance. Crawling traverses  $1\text{--}2$  cells per action (each  $0.5 \times 0.5$  m), biped follows the same formulation, and rolling is constrained to exactly 3 cells per action.

We first fix the trajectory horizon  $T$  and vary all remaining hyperparameter (weight on exploration, weight on goal, epsilon, and Big-M constant), selecting the two configurations that minimize EVC while always reaching the goal. The objective weights  $W_{\text{exp}}$  and  $W_{\text{goal}}$  balance exploration and goal-reaching, while  $\epsilon$  and  $M$  define the Big-M constraint. We found that low EVC is achieved when exploration and goal objectives are equally balanced, with  $\epsilon$  and  $M$  both low or both high, and an average mode-switch rate of approximately

TABLE III: Energy Consumption per Visited Cell for Each Mode

Mode	Energy/Visited Cells (J/cell)
Biped	26.89
Crawl	5.11
Roll	21.96

25% per time step.

We also tested the case where all parameters (including  $T$ ) are varied but the robot is restricted to a single locomotion mode, Table III. Mode-specific regions from Fig. 7 are excluded, and only obstacle constraints are enforced. In this test, we found that crawling achieves the lowest EVC (5.11 J/cell), outperforming bipedal (26.89 J/cell) and rolling locomotion (21.96 J/cell). Rolling reaches the goal fastest ( $T = 15$ ) due to its higher speed, but provides limited coverage: only one cell is counted as visited during rolling due to onboard sensor limitations, a constraint enforced in the MIQCP formulation. Biped locomotion exhibits the highest failure rate, as its limited per-step distance requires longer horizons, increasing optimization difficulty. Although biped mode offers greater coverage than rolling, it is substantially less energy-efficient due to higher energy expenditure per step.

Overall, crawling provides the most favorable trade-off between energy efficiency and grid coverage, while rolling prioritizes traversal speed. Biped locomotion is less energy-efficient than crawling. Using realistic COM heights, biped motion requires approximately 104 J/m compared to 65 J/m for crawling, primarily due to increased potential energy costs and higher per-actuator loads. Crawling distributes both kinetic and control effort across more limbs, reducing peak actuator loads

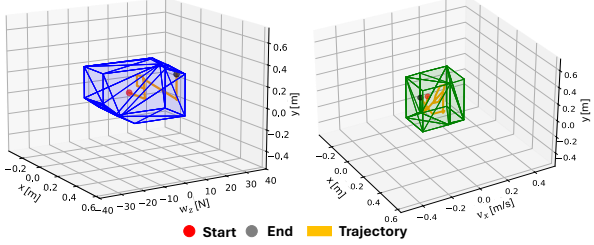


Fig. 9: Example visual representation of the Maximal Output Admissible Set (MOAS), Sec. IV-B1. The trajectory on the left represents a 3D state from estimation following the reference in Fig. 10, where  $x$  and  $y$  denote end-effector position,  $w_z$  the wrench, and  $v_x$  the linear velocity.

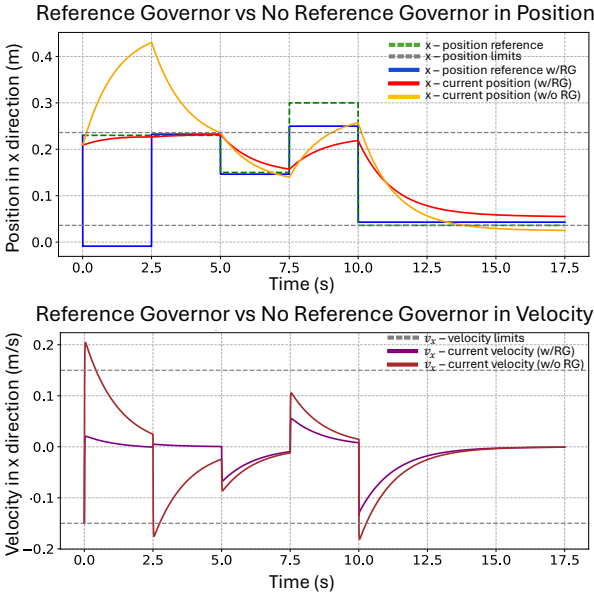


Fig. 10: End-effector  $x$ -position and velocity tracking with and without a reference governor. Position (top) and velocity (bottom) constraints are indicated by dashed lines.

and improving thermal efficiency. Further analysis, including hyperparameter selection, and energy comparisons are given in Tables V and VI of Appendix.

#### F. Vertical Mobility

1) *Vertical Climbing on a Kid's Slide*: Leveraging MOBIUS's multi-modal locomotion and spine-enhanced grippers, MOBIUS can climb a children's slide, as shown in Fig. 1d. The robot pinch-grasps the side rails while stepping upward and subsequently slides down head-first after reaching the top. Across ten trials, eight were successful; failures occurred when a foot failed to advance to the next step (e.g., toe entrapment). A visual-servo controller aligns the end-effectors to the vertical handles (Fig. 1f), after which an open-loop trajectory is executed for climbing and descent, demonstrating hardware capability even without closed-loop control for the robot base. Note, we provide the full visual sequence of climbing the ladder in Fig. 10 of Appendix.

2) *Pinch Grasp Pull-up*: The pinch grasp pull-up task demonstrates the strength and compliance of MOBIUS's

forearm and gripper design (Fig. 1e). MOBIUS pinch-grasps aluminum structural bars and lifts its full body from a straight-arm dead-hang configuration. The uniform limb design provides effective load distribution, which is critical for climbing, while admittance control in the forearms enables compliant motion during the pull-up. Spine tips are typically effective on rough surfaces with microcavities; however, in the pull-up task (Fig. 1e), they also support MOBIUS's full body weight on an aluminum bar while executing admittance control. The spines engage grooves parallel to the bar, producing a limit surface that bounds the maximum grasping force (Table IV). The grasp generates a dominant shear force of 124.2 N perpendicular to the groove ( $z$ -axis), while frictional force along the groove ( $x$ -axis) remains low at 23.6 N. Although the spine limit surface is stochastic, the  $z$ -axis force exhibits a higher standard deviation (24.5 N) than the  $x$ -axis (4.1 N), indicating that spine engagement, rather than friction, dominates load support, enabling a single gripper to sustain MOBIUS's weight in the  $z$  direction.

TABLE IV: Maximum supporting force of the spine gripper on a slippery aluminum bar in Fig. 1e.

Direction	Maximum Supporting Force
$x$ -axis	23.6 N $\pm$ 4.1 N
$z$ -axis	124.2 N $\pm$ 24.5 N

3) *Auto-Tuning Admittance Control and Safety Analysis*: Manual tuning of the admittance force controller for the pull-up task is difficult due to end-effector constraints and the arms supporting the robot's full body weight. Auto-tuning improves force tracking error by 45% while maintaining controller stability, consistent with results reported from Schperberg et al. [31]. Safety during force control is enforced using the Reference Governor (RG) described in Sec. IV-B1. Figs. 9 and 10 illustrate these guarantees. Fig. 9 shows the MOAS during force control while tracking the position in Fig. 10 with a reference wrench of 0 N. The system trajectory (yellow), from the initial state (red) to the final state (gray), remains entirely within the admissible set, ensuring safety. Fig. 10 compares end-effector motion with and without RG. The  $x$  position with RG (red) remains within kinematic limits (gray dashed), whereas without RG (yellow) it violates these constraints. The RG modifies the reference (blue) only when necessary; for example, from 10.0 to 17.5 s, the reference is unchanged as the trajectory stays within the MOAS. The lower plot shows that RG enforces velocity limits: the end-effector velocity with RG (purple) remains within bounds, while without RG (dark red) violations occur at 0.0 s 2.5 s, and 10.0 s. Additional results showing force tracking are provided in Sec. F of Appendix.

#### G. Conclusion and Limitations

We demonstrated that MOBIUS achieves bipedal walking, crawling, rolling, and dynamic climbing, including pinching-based pull-ups. The system combines a compact, fatigue-resistant hardware design with high-DoF limbs and a cohesive

control stack integrating model-free RL, admittance force control, and MIQCP-based high-level decision making. Extensive simulation and hardware experiments validate the value of co-designing morphology, control, and planning.

Despite its versatility, MOBIUS involves several trade-offs. The dual use of grippers for grasping and locomotion increases mechanical complexity and wear, while spur gears are susceptible to fatigue under high-impact bipedal loads. The reinforcement learning controllers depend on extensive domain randomization and may generalize poorly to novel surfaces, and state estimation for rolling is unreliable. In addition, the MIQCP-based planner operates offline with assumed terrain knowledge, limiting real-time reactivity, and bipedal locomotion remains energy-intensive. Future work will address real-time replanning, long-horizon autonomy in cluttered environments, language-conditioned task specification, and hardware refinements for energy efficiency and outdoor deployment.

## REFERENCES

[1] Xinpei Ai, Hengmao Yue, and Wei Dawid Wang. Crawling soft robot exploiting wheel-legs and multimodal locomotion for high terrestrial maneuverability. *IEEE Transactions on Robotics*, 39(6):4230–4239, 2023. doi: 10.1109/TRO.2023.3299530.

[2] Max P Austin, Jason M Brown, Charles A Young, and Jonathan E Clark. Leg design to enable dynamic running and climbing on bobcat. In *2018 IEEE/RSJ International Conference on Intelligent Robots and Systems*, pages 3799–3806. IEEE, 2018.

[3] Guillaume Bellegarda, Yiyu Chen, Zhuochen Liu, and Quan Nguyen. Robust high-speed running for quadruped robots via deep reinforcement learning. In *2022 IEEE/RSJ International Conference on Intelligent Robots and Systems (IROS)*, pages 10364–10370, 2022. doi: 10.1109/IROS47612.2022.9982132.

[4] Marko Bjelonic, C. Dario Bellicoso, Yvain de Viragh, Dhionis Sako, F. Dante Tresoldi, Fabian Jenelten, and Marco Hutter. Keep rollin’—whole-body motion control and planning for wheeled quadrupedal robots. *IEEE Robotics and Automation Letters*, 4(2):2116–2123, 2019. doi: 10.1109/LRA.2019.2899750.

[5] Amanda Bouman, Muhammad Fadhil Ginting, Nikhilesh Alatur, Matteo Palieri, David D. Fan, Thomas Touma, Torkom Pailevanian, Sung-Kyun Kim, Kyohei Otsu, Joel Burdick, and Ali-akbar Agha-Mohammadi. Autonomous spot: Long-range autonomous exploration of extreme environments with legged locomotion. In *2020 IEEE/RSJ International Conference on Intelligent Robots and Systems (IROS)*, pages 2518–2525, 2020. doi: 10.1109/IROS45743.2020.9341361.

[6] Timothy Bretl. Motion planning of multi-limbed robots subject to equilibrium constraints: The free-climbing robot problem. *The International Journal of Robotics Research*, 25(4):317–342, 2006.

[7] Guillermo A. Castillo, Bowen Weng, Wei Zhang, and Ayonga Hereid. Robust feedback motion policy design using reinforcement learning on a 3d digit bipedal robot. In *2021 IEEE/RSJ International Conference on Intelligent Robots and Systems (IROS)*, pages 5136–5143, 2021. doi: 10.1109/IROS51168.2021.9636467.

[8] Zhe Chen, Brandon Tighe, and Jianguo Zhao. Origami-inspired modules enable a reconfigurable robot with programmable shapes and motions. *IEEE/ASME Transactions on Mechatronics*, 27(4):2016–2025, 2022. doi: 10.1109/TMECH.2022.3175145.

[9] Lillian Chin, Max Burns, Gregory Xie, and Daniela Rus. Flipper-style locomotion through strong expanding modular robots. *IEEE Robotics and Automation Letters*, 8(2):528–535, 2023. doi: 10.1109/LRA.2022.3227872.

[10] Pravin Dangol, Eric Sihite, and Alireza Ramezani. Control of thruster-assisted, bipedal legged locomotion of the harpy robot. *Frontiers in Robotics and AI*, 8, 2021. ISSN 2296-9144. doi: 10.3389/frobt.2021.770514. URL <https://www.frontiersin.org/articles/10.3389/frobt.2021.770514>.

[11] Alejandro Escontrela, Xue Bin Peng, Wenhao Yu, Tingnan Zhang, Atil Iscen, Ken Goldberg, and Pieter Abbeel. Adversarial motion priors make good substitutes for complex reward functions, 2022. URL <https://arxiv.org/abs/2203.15103>.

[12] Siyuan Feng, X Xinjilefu, Christopher G. Atkeson, and Joohyung Kim. Optimization based controller design and implementation for the atlas robot in the darpa robotics challenge finals. In *2015 IEEE-RAS 15th International Conference on Humanoid Robots (Humanoids)*, pages 1028–1035, 2015. doi: 10.1109/HUMANOIDS.2015.7363480.

[13] Zipeng Fu, Xuxin Cheng, and Deepak Pathak. Deep whole-body control: Learning a unified policy for manipulation and locomotion. In *Conference on Robot Learning (CoRL)*, 2022.

[14] Yifeng Gong, Ge Sun, Aditya Nair, Aditya Bidwai, Raghuram CS, John Grezmar, Guillaume Sartoretti, and Kathryn A. Daltorio. Legged robots for object manipulation: A review. *Frontiers in Mechanical Engineering*, 9, 2023. ISSN 2297-3079. doi: 10.3389/fmech.2023.1142421.

[15] Yukai Gong, Ross Hartley, Xingye Da, Ayonga Hereid, Omar Harib, Jiunn-Kai Huang, and Jessy Grizzle. Feedback control of a cassie bipedal robot: Walking, standing, and riding a segway. In *2019 American Control Conference (ACC)*, pages 4559–4566, 2019. doi: 10.23919/ACC.2019.8814833.

[16] Gurobi Optimization, LLC. Gurobi Optimizer Reference Manual, 2024. URL <https://www.gurobi.com>.

[17] Joshua Hooks, Min Sung Ahn, Jeffrey Yu, Xiaoguang Zhang, Taoyuanmin Zhu, Hosik Chae, and Dennis Hong. Alphred: A multi-modal operations quadruped robot for package delivery applications. *IEEE Robotics and Automation Letters*, 5(4):5409–5416, 2020. doi: 10.1109/LRA.2020.3007482.

[18] Marco Hutter, Christian Gehring, Dominic Jud, Andreas

Lauber, C Dario Bellicoso, Vassilios Tsounis, Jemin Hwangbo, Karen Bodie, Peter Fankhauser, Michael Bloesch, et al. Anymal-a highly mobile and dynamic quadrupedal robot. In *2016 IEEE/RSJ international conference on intelligent robots and systems*, pages 38–44. IEEE, 2016.

[19] Kyunam Kim, Patrick Spieler, Elena-Sorina Lupu, Alireza Ramezani, and Soon-Jo Chung. A bipedal walking robot that can fly, slackline, and skateboard. *Science Robotics*, 6(59):eabf8136, 2021. doi: 10.1126/scirobotics.abf8136. URL <https://www.science.org/doi/abs/10.1126/scirobotics.abf8136>.

[20] Sangbae Kim, Matthew Spenko, Salomon Trujillo, Barrett Heyneman, Daniel Santos, and Mark R Cutkosky. Smooth vertical surface climbing with directional adhesion. *IEEE Transactions on robotics*, 24(1):65–74, 2008.

[21] Korea Atomic Energy Research Institute. Korea atomic energy research institute (kaeri) — english website. <https://www.kaeri.re.kr/eng/>, 2025. Accessed: 31 Oct. 2025.

[22] Scott Kuindersma, Frank Permenter, and Russ Tedrake. An efficiently solvable quadratic program for stabilizing dynamic locomotion. In *2014 IEEE International Conference on Robotics and Automation (ICRA)*, pages 2589–2594, 2014. doi: 10.1109/ICRA.2014.6907230.

[23] Kenji Nagaoka, Hayato Minote, Kyohei Maruya, Yuki Shirai, Kazuya Yoshida, Takeshi Hakamada, Hirotaka Sawada, and Takashi Kubota. Passive spine gripper for free-climbing robot in extreme terrain. *IEEE Robotics and Automation Letters*, 3(3):1765–1770, 2018.

[24] Aaron Parness, Neil Abcouwer, Christine Fuller, Nicholas Wiltzie, Jeremy Nash, and Brett Kennedy. Lemur 3: A limbed climbing robot for extreme terrain mobility in space. In *2017 IEEE international conference on robotics and automation*, pages 5467–5473. IEEE, 2017.

[25] Giulia Piovan and Francesco Bullo. On coordinate-free rotation decomposition: Euler angles about arbitrary axes. *IEEE Transactions on Robotics*, 28(3):728–733, 2012. doi: 10.1109/TRO.2012.2184951.

[26] Max Polzin, Qinghua Guan, and Josie Hughes. Robotic locomotion through active and passive morphological adaptation in extreme outdoor environments. *Science Robotics*, 10(99):eadp6419, 2025. doi: 10.1126/scirobotics.adp6419. URL <https://www.science.org/doi/abs/10.1126/scirobotics.adp6419>.

[27] Marc H. Raibert. *Legged Robots That Balance*. Massachusetts Institute of Technology, USA, 1986. ISBN 0262181177.

[28] Marc H. Raibert, Jr H. Benjamin Brown, and Michael Chepponis. Experiments in balance with a 3d one-legged hopping machine. *The International Journal of Robotics Research*, 3(2):75–92, 1984. doi: 10.1177/027836498400300207. URL <https://doi.org/10.1177/027836498400300207>.

[29] Joseph Redmon, Santosh Divvala, Ross Girshick, and Ali Farhadi. You only look once: Unified, real-time object detection. In *2016 IEEE Conference on Computer Vision and Pattern Recognition (CVPR)*, pages 779–788, 2016. doi: 10.1109/CVPR.2016.91.

[30] Aaron Saunders, Daniel I Goldman, Robert J Full, and Martin Buehler. The rise climbing robot: body and leg design. In *Unmanned Systems Technology VIII*, volume 6230, pages 401–413. SPIE, 2006.

[31] Alexander Schperberg, Yuki Shirai, Xuan Lin, Yusuke Tanaka, and Dennis Hong. Adaptive force controller for contact-rich robotic systems using an unscented kalman filter. In *2023 IEEE-RAS 23rd International Conference on Humanoid Robots*, 2023.

[32] Alexander Schperberg, Yusuke Tanaka, Saviz Mowlavi, Feng Xu, Bharathan Balaji, and Dennis Hong. Optistate: State estimation of legged robots using gated networks with transformer-based vision and kalman filtering. *arXiv preprint arXiv:2401.16719*, 2024.

[33] Alexander Schperberg, Yiping Wang, and Stefano Di Cairano. Safe whole-body loco-manipulation via combined model and learning-based control. In *Proceedings of the IEEE International Conference on Robotics and Automation (ICRA)*, Vienna, Austria, 2026. To appear.

[34] Sangok Seok, Albert Wang, Meng Yee Chuah, David Otten, Jeffrey Lang, and Sangbae Kim. Design principles for highly efficient quadrupeds and implementation on the mit cheetah robot. In *2013 IEEE International Conference on Robotics and Automation*, pages 3307–3312. IEEE, 2013.

[35] Fan Shi, Timon Homberger, Joonho Lee, Takahiro Miki, Moju Zhao, Farbod Farshidian, Kei Okada, Masayuki Inaba, and Marco Hutter. Circus anymal: A quadruped learning dexterous manipulation with its limbs. In *2021 IEEE International Conference on Robotics and Automation*, pages 2316–2323. IEEE, 2021.

[36] Manjia Su, Yu Qiu, Yisheng Guan, Haifei Zhu, and Zhi Liu. Climbot-Ω: A soft robot with novel grippers and rigid-compliantly constrained body for climbing on various poles. In *2021 IEEE/RSJ International Conference on Intelligent Robots and Systems*, pages 4975–4981. IEEE, 2021.

[37] Yusuke Tanaka, Yuki Shirai, Zachary Lacey, Xuan Lin, Jane Liu, and Dennis Hong. An under-actuated whipple-tree mechanism gripper based on multi-objective design optimization with auto-tuned weights. In *2021 IEEE/RSJ International Conference on Intelligent Robots and Systems*, pages 6139–6146, 2021. doi: 10.1109/IROS51168.2021.9635872.

[38] Yusuke Tanaka, Yuki Shirai, Xuan Lin, Alexander Schperberg, Hayato Kato, Alexander Swerdlow, Naoya Kummagai, and Dennis Hong. Scaler: A tough versatile quadruped free-climber robot. In *2022 IEEE/RSJ International Conference on Intelligent Robots and Systems*, pages 5632–5639, 2022. doi: 10.1109/IROS47612.2022.9981555.

[39] Emanuel Todorov, Tom Erez, and Yuval Tassa. MuJoCo: A physics engine for model-based control. In

2012 IEEE/RSJ International Conference on Intelligent Robots and Systems, pages 5026–5033. IEEE, 2012. doi: 10.1109/IROS.2012.6386109.

- [40] Vassilios Tsounis, Mitja Alge, Joonho Lee, Farbod Farshidian, and Marco Hutter. Deepgait: Planning and control of quadrupedal gaits using deep reinforcement learning. *IEEE Robotics and Automation Letters*, 5(2): 3699–3706, 2020. doi: 10.1109/LRA.2020.2979660.
- [41] Kentaro Uno, Naomasa Takada, Taku Okawara, Keigo Haji, Arthur Candalot, Warley F. R. Ribeiro, Kenji Nagaoka, and Kazuya Yoshida. Hubrobo: A lightweight multi-limbed climbing robot for exploration in challenging terrain. In *2020 IEEE-RAS 20th International Conference on Humanoid Robots (Humanoids)*, pages 209–215, 2021. doi: 10.1109/HUMANOID\$47582.2021.9555799.
- [42] Eric Vollenweider, Marko Bjelonic, Victor Klemm, Nikita Rudin, Joonho Lee, and Marco Hutter. Advanced skills through multiple adversarial motion priors in reinforcement learning. In *2023 IEEE International Conference on Robotics and Automation (ICRA)*, pages 5120–5126, 2023. doi: 10.1109/ICRA48891.2023.10160751.
- [43] Justin K. Yim and Ronald S. Fearing. Precision jumping limits from flight-phase control in salto-1p. pages 2229–2236, 2018. doi: 10.1109/IROS.2018.8594154.
- [44] Chen Yu and Andre Rosendo. Multi-modal legged locomotion framework with automated residual reinforcement learning. *IEEE Robotics and Automation Letters*, 7(4):10312–10319, 2022. doi: 10.1109/LRA.2022.3191071.